JOURNAL OF MATERIALS SCIENCE **39** (2004) 2303–2314

Effect of iron and manganese contents on convection-free precipitation and sedimentation of primary α-Al(FeMn)Si phase in liquid Al-11.5Si-0.4Mg alloy

X. CAO
Aerospace Manufacturing Technology Centre, Institute for Aerospace Research, National Research Council Canada, 3385 Griffith Street, St.-Laurent, Quebec, H4T 1W5, Canada
E-mail: Xinjin.Cao@cnrc-nrc.gc.ca

N. SAUNDERS
Thermotech Ltd., Surrey Technology Centre, The Surrey Research Park, Guildford, Surrey GU2 7YG, United Kingdom
E-mail: Nigel.Saunders@thermotech.co.uk

J. CAMPBELL
Department of Metallurgy and Materials, The University of Birmingham, B15 2TT, United Kingdom
E-mail: J.Campbell.Met@bham.ac.uk

The effect of Fe and Mn contents on precipitation and sedimentation of primary α-Al(FeMn)Si phase in liquid Al-11.5Si-0.4Mg (wt%) alloy has been investigated at 600°C in convection-free conditions. Almost all primary α-Al(FeMn)Si particles and some oxide films seem to completely settle to the base of the melts. With the increase of original iron equivalent values (IEV) or Mn/Fe ratio at a given Fe level there are increases in particle weight, number and size. The particle volume fraction and depth of sediment also increase with IEV or Mn/Fe ratio at a given iron level. However, the particle volume fraction and average sizes probably remain plateaus with IEVs from 2 to 5.5. There is an equilibrium Mn content corresponding to a precipitation temperature for a given alloy. In Al-11.5Si-0.4Mg alloy containing 0.7–1.22Fe and 0.3–2.15Mn, Mn is approximately 0.3% after sedimentation at 600°C. The removal efficiency of Fe and Mn increases with original IEV or Mn/Fe ratio at a given Fe level. Mn has higher removal efficiency than Fe. Experimental results for primary particle amounts and compositions were compared to predictions from software JMatPro. Good agreement was found suggesting that the modelling route could be used to explore different alloys where sedimentation would take place.

1. Introduction

Casting quality is primarily influenced by the casting process and subsequent treatments such as heat treatment, hot isostatic pressing (HIPing), etc. Casting techniques developed to improve the quality of cast aluminium alloys can be categorized as (i) control of the liquid metal quality prior to casting; (ii) control of the pouring of liquid metal into a mould; and (iii) control of casting microstructures and defects during solidification. Because of the commercial and technological importance of cast aluminium alloys, these processes have been the subjects of extensive research for several decades aimed at improving the quality of cast alloys.

Unfortunately, liquid aluminium is usually laden with entrained oxide films. The entrainment process ensures that the films are doubled-over and frozen into castings as cracks. If care is not taken to remove oxide films suspended in the melts, they can lead to a variety of problems [1, 2]: (i) loss of fluidity and feeding properties such that the amount of microporosity may increase; (ii) increase in gas porosity with gas-coated films acting as sites for heterogeneous initiation of gas or shrinkage cavities; (iii) increase in the tendency for hot tearing because oxide films may act as sites for the heterogeneous nucleation of hot tears; (iv) leakage defects resulting from folded oxide films providing leakage paths by connecting wall to wall of castings, with bubble trails and non-wetted confluences of melt fronts being also particularly troublesome with respect to leak-tightness; (v) poor machinability giving increasing tool wear and poor surface finish because

of the extreme hardness of oxides; and (vi) reduction in the mechanical properties and reliability of castings because oxide films as cracks in castings introduce structural weakness, causing reduction and scatter of strength, ductility, and fatigue resistance, etc. In summary, therefore, the entrained oxide cracks are a source of concern because they are often not detectable by normal non-destructive testing techniques but are highly damaging to casting quality.

Over recent years the separation and removal of oxide films from aluminium melts has been a key research field. Basically, there are four techniques currently used to clean molten aluminium alloys: sedimentation, fluxing, degassing (flotation), and filtration [3, 4]. Success, however, using these conventional methods has been mixed. A new technique, termed the heat treatment of liquid metal (precipitation and sedimentation of primary intermetallic compounds from melts), has been explored to remove both oxide films and primary intermetallic compounds from the aluminium melt [5–12]. The concept was to remove oxide crack defects from liquid metal by precipitation of primary intermetallic compounds onto the oxide films, causing them to sink under the weight of the particles. The intermetallic compounds, especially primary $Al_{15}(FeMn)_3Si_2$ or $Al_{15}(FeMnCr)_3Si_2$ (commonly termed sludge, here referred to as primary α-Al(FeMn)Si), appeared to precipitate onto the wetted outer interfaces of double oxide films [5–12].

The precipitation and separation of primary $Al_{15}(FeMn)_3Si_2$ or $Al_{15}(FeMnCr)_3Si_2$ from melts is often experienced in aluminium foundries, especially in the pressure diecasting industry where low melt holding and casting temperatures are typical and compositions with high Fe, Mn and Cr levels are often employed [13]. Preliminary investigation into the heat treatment of Al-11.5Si-0.4Mg-0.57Fe-0.59Mn-0.17Ti alloy precipitated at 600°C for 10 min showed a clear improvement in the cleanness of the melts, which in turn was associated with an increase in the tensile properties and reliability of the castings [5, 8]. Thus the precipitation and separation of primary intermetallics appeared to be capable of removing both iron and oxides from aluminium melts. It seems likely that the removal efficiency of oxide films could be related to the amount of primary α-Al(FeMn)Si particles precipitated in aluminium melts. Therefore, if the reduction of oxides is to be understood, it is important to investigate the influence of Fe and Mn contents on the precipitation and sedimentation of the primary α-Al(FeMn)Si phase. Little work appears to have been reported in this field.

In this work, a convection-free technique has been specially developed to sediment the primary α-Al(FeMn)Si particles as completely as possible. Thus the paper reports on the effect of iron and manganese contents on the precipitation and sedimentation of primary α-Al(FeMn)Si phase in cast Al-11.5Si-0.4Mg alloys in convection-free conditions.

2. Experimental procedures

The material used in this research was a commercial aluminium-silicon alloy LM9 (UK designation). The specified and actual compositions of the experimental alloy are compared in Table I. The alloy is approximately of eutectic composition, which has the advantage that the melt can be cooled to lower temperatures to facilitate precipitation of primary α-Al(FeMn)Si particles. A second reason for the choice of this alloy was that it has relatively high Fe and Mn contents, thus it is expected that the experimental alloy with Fe and Mn contents originally above specification would have its chemical composition within specification after precipitation processing. The experimental material was prepared from Al-30Si, Al-4Fe and Al-10Mn hardener alloys, 99.8% magnesium and 99.89% aluminium. The Al-4Fe master alloy was melted from 99.88% iron and 99.89% aluminium, and the Al-30Si from 98.7% silicon and 99.89% aluminium. The Al-10Mn was a commercial master alloy.

Prior to melting, a clay-graphite crucible (capacity 3 kg) was preheated in a muffle furnace at 450°C (842°F) overnight. A mass of 3 kg of the experimental alloy was charged to the preheated crucible, melted in an induction furnace, heated to 760°C (1400°F) and held for 20 min at this temperature to fully dissolve the charges. Hydrogen content in the melt just prior to pouring was measured using a Severn Science unit. The melting crucible was then lifted together with its molten charge from the induction coil and the liquid metal was poured into a stainless steel mould. Disc-shaped chemical analysis samples were taken from the remainder of the liquid metal by casting into a metal die.

The mould, with an inner diameter of approximately 20 mm, outside diameter 25.4 mm and length of 210 mm, was made from 316 stainless steel tube. The bottom of the tube was closed by welding on a plate of identical material using tungsten-arc inert gas (TIG) welding. To avoid dissolution of the stainless steel and

TABLE I Chemical compositions of Al-11.5Si-0.4Mg (LM9) alloy used in the present work

Alloys	Si	Mg	Fe	Mn	Ti	Cr	Cu	Ni	Zn	Pb	Sn	Al	IEV
Specification	10.0–13.0	0.2–0.6	0.6[a]	0.3–0.7	0.2[a]		0.1[a]	0.1[a]	0.1[a]	0.1[a]	0.05[a]	Balance	
1	11.29	0.38	0.70	0.59	0.01	0.02	0.02	0.03	0.02	0.007	<0.005	Balance	1.94
2	11.59	0.37	1.16	0.29	0.02	0.002	0.02	0.02	0.01	0.002	<0.005	Balance	1.75
3	11.49	0.35	1.08	0.50	0.02	0.002	0.02	0.03	0.03	<0.005	<0.005	Balance	2.09
4	11.92	0.39	1.23	1.11	0.02	0.006	0.04	0.03	0.04	<0.005	<0.005	Balance	3.47
5	11.69	0.35	1.22	2.15	0.02	0.005	0.06	0.03	0.04	0.027	<0.005	Balance	5.54

Alloy compositions given in wt% unless noted otherwise.
[a]Maximum value. Iron equivalent value (IEV) = 1 Fe + 2 Mn + 3 Cr (%).

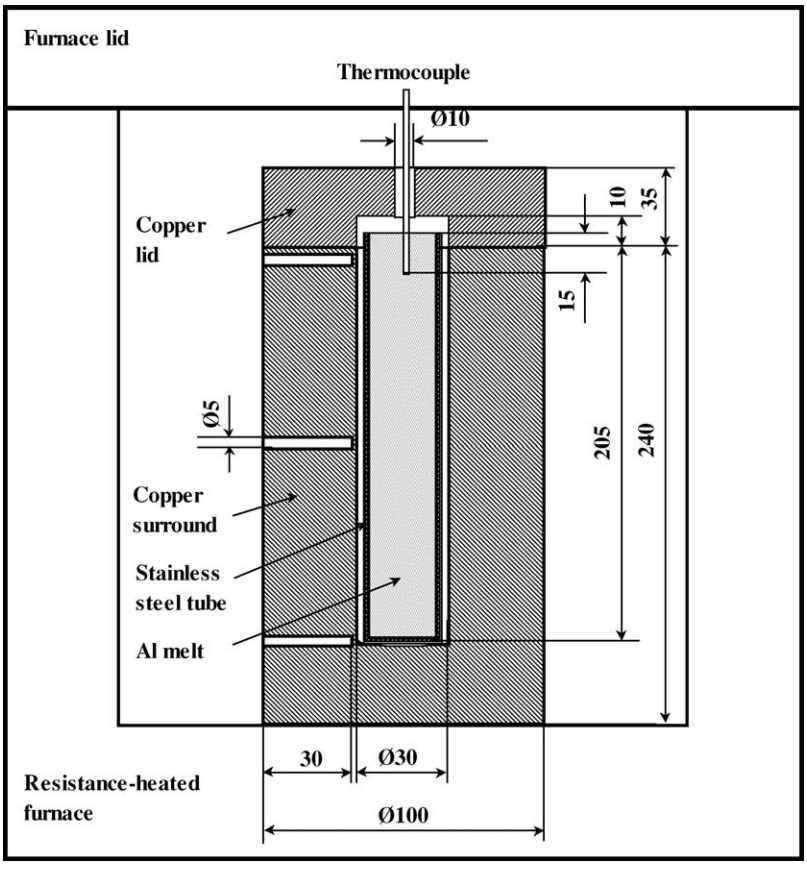

Figure 1 Experimental set-up used for convention-free sedimentation. Dimensions shown are in mm.

interaction between the mould and liquid metal during holding, the mould was coated with a wash of boron nitride. It was then naturally dried for a few days at room temperature, baked at 200°C (392°F), and finally preheated to 800°C (1472°F) for at least 30 min to reduce hydrogen pickup by the melt. The melt at 760°C (1400°F) was poured into the mould at 800°C, and the mould was then quickly transferred into a massive copper die (made from 99.99Cu). The copper die had been held at 600°C (1112°F) in a resistance-heated holding furnace. The quick transfer was needed to avoid solidification of the melt in the stainless steel mould prior to precipitation. The heavy copper surround to the stainless steel mould reduced temperature variations in the melt, and so reduced the driving force for natural convection. Fig. 1 shows a cross section of the mould and copper surround in the holding furnace.

The liquid metal was held at 600°C in its convection-free environment for 4 h to allow the full sedimentation of primary α-Al(FeMn)Si particles and oxide films. During the course of precipitation, a K-type thermocouple was inserted into the liquid metal at a depth of around 15 mm from the top of the melt to monitor the temperature of the melt. Another three K-type thermocouples were also inserted into the copper die at or near the top, middle and bottom of the stainless steel mould to monitor temperature differences during holding. Typical temperatures were 605 (1121), 603 (1117), 602°C (1116°F), respectively.

After 4 h, the power supply of the resistance-heated holding furnace was switched off, and the liquid metal was then slowly cooled from 600°C to room temperature. No transfer or other actions such as water quenching were taken to avoid any possible mechanical disturbance that may have stirred the precipitates. The cooling and solidification was monitored by the 15 mm deep thermocouple at the top of the mould. The readings were logged at 50 readings per second into a file by an Apple Macintosh IIci using a program written in Labview graphical programming environment to drive a National Instruments NB-MIO-16H acquisition card.

The metal sample after solidification, with an average weight of approximate 142 g and a length of approximately 200 mm, was taken out from the stainless steel mould, and then sectioned longitudinally. One half of the sample was used for chemical analysis along the length of the casting using glow discharge spectrometry. The other half of the casting was used for metallographic observations. The half casting was cut into small pieces, each with section area 20 × 20 mm. The pieces were mounted and polished to a 1 μm diamond finish. Polishing was completed using magnesia powder to produce a mirror-like finish. The polished samples were then etched in 0.8% HF solution. The microstructures were studied using Leica optical microscopy and JEOL6300 scanning electron microscopy (SEM), while the primary α-Al(FeMn)Si particles were measured using a Leica Cambridge Ltd. image analysis system, and an optical microscope equipped with Quantimet 500 Qwin (Version V02.00A). The measurements included the area percentage of primary α-Al(FeMn)Si particles, average sizes, particle numbers per unit area, and shape factors such as aspect ratio,

fullness ratio and roundness. The aspect ratio is the ratio of Length (the length of the longest feret) divided by Breadth (the length of the shortest feret). The fullness ratio is a shape factor, equal to the square root of the ratio of area to circumscribed area (Fullness Ratio = (Area/Convex Area)$^{1/2}$, which has a maximum value of unity for a circle). The roundness is also a shape factor that is calculated from the ratio of perimeter squared to the area (Roundness = Perimeter^2/(4 $\times$ π $\times$ Area $\times$ 1.064)). The adjustment factor of 1.064 corrects the perimeter for the effect of the corners produced by the digitisation of the image. The roundness gives a minimum value of unity for a circle. The average sizes of primary α-Al(FeMn)Si particles were measured in two ways: equivalent circle diameter (i.e., the diameter of a circle having the same area as the feature) and feret diameter (i.e., the maximum spacing between parallel tangents to a feature in a given direction). The feret is equivalent to the diameter measured using a pair of callipers. The feret size for each particle was the average of eight measurements at 0°, 22.5°, 45°, 67.5°, 90°, 112.5°, 135° and 157.5°. The reported average equivalent circle and feret diameters were statistically calculated from all measurements of primary α-Al(FeMn)Si particles for each casting. It is noted that some primary intermetallics sparsely distributed close to or on the mould wall above the precipitate-rich metal were omitted because of their scattered amount and location. However, this omission is estimated to have an insignificant effect on the results. All the reported results were taken from the average measurements of about 20 fields at a magnification of 100 ("field" representing the field of view of the optical microscope and covering an area inside a diameter of approximately 1.17 mm).

The number of particles per unit volume was calculated from the number of particles per unit area divided by average particle diameter (in this case equivalent circle diameter) [14, 15]. Because the primary intermetallics were sedimented fully to the bottom of the castings (apart from a few clusters that had become attached to the side of the mould or the very top of the castings), the total number of particles was estimated from the number of particles per unit volume in the precipitate-rich castings. The number of primary intermetallics for each gram of the alloy was calculated from the total number of particles divided by the total weight of each casting. The precipitated particle weight was estimated from the total number of particles multiplied by particle volume and density. The precipitated particle weight percentage was obtained from the particle weight divided by the whole weight of each casting.

The estimated weight of primary α-Al(FeMn)Si phase (here identified as "Experimental") has been contrasted with modelled results using the software programme JMatPro (JMatPro is an acronym for Java based Materials Property software) [16, 17]. In the work the JMatPro software has also been used to calculate alloy thermophysical properties and thermodynamics, compositions of primary α-Al(FeMn)Si phase and alloy chemistry after sedimentation processing.

3. Results

The liquid metal prior to pouring had an average hydrogen content of 0.24 cm^3/100 g Al. Metallurgical observations showed that precipitation and sedimentation of primary intermetallics occurred at 600°C for all the experimental alloys. After 4-h sedimentation it was found that there are some primary α-Al(FeMn)Si intermetallic particles on or near the stainless steel mould wall randomly scattered at various heights. Fig. 2 shows some primary α-Al(FeMn)Si particles of Alloy 2 casting distributed on or close to the mould wall. The primary α-Al(FeMn)Si particles and some oxide films near the central axis of the castings appear to have fully settled to the bottom of the mould. Fig. 3 shows oxide films and primary α-Al(FeMn)Si particles at the bottom of Alloy 2 casting. Fig. 4 shows the distribution of primary α-Al(FeMn)Si particles at different heights of the Alloy 5 casting. Fig. 5 shows the variation of the depth of precipitate-rich metal in the stainless steel mould with the iron equivalent values (IEV) of the original alloys. Fig. 6a shows the effect of original Fe and Mn contents on area percentage of primary α-Al(FeMn)Si particles along the length of the castings, while Fig. 6b shows the effect of the IEV of original alloys on the

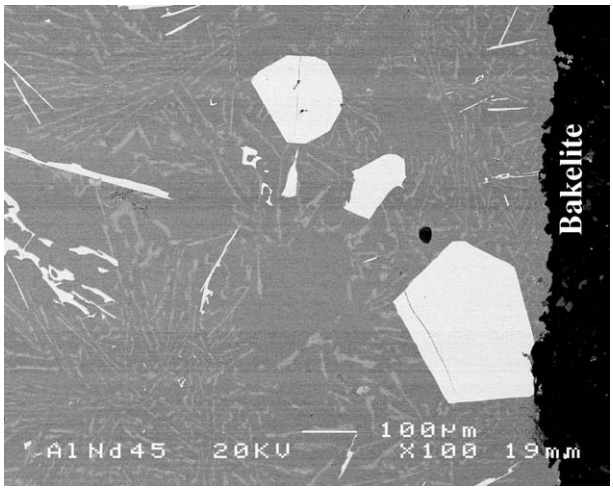

Figure 2 Back-scattered electron image taken at 70 mm from the base of Alloy 2 casting sedimented at 600°C for 4 h showing primary α-Al(FeMn)Si particles on or near the stainless steel mould wall.

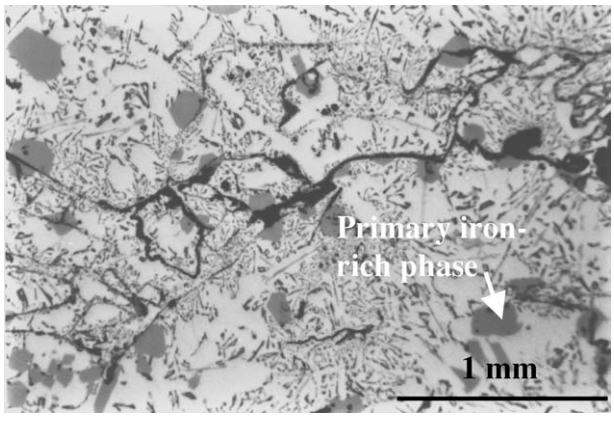

Figure 3 Optical micrograph of Alloy 2 casting sedimented at 600°C for 4 h showing oxide films and primary α-Al(FeMn)Si particles at the base of the casting.

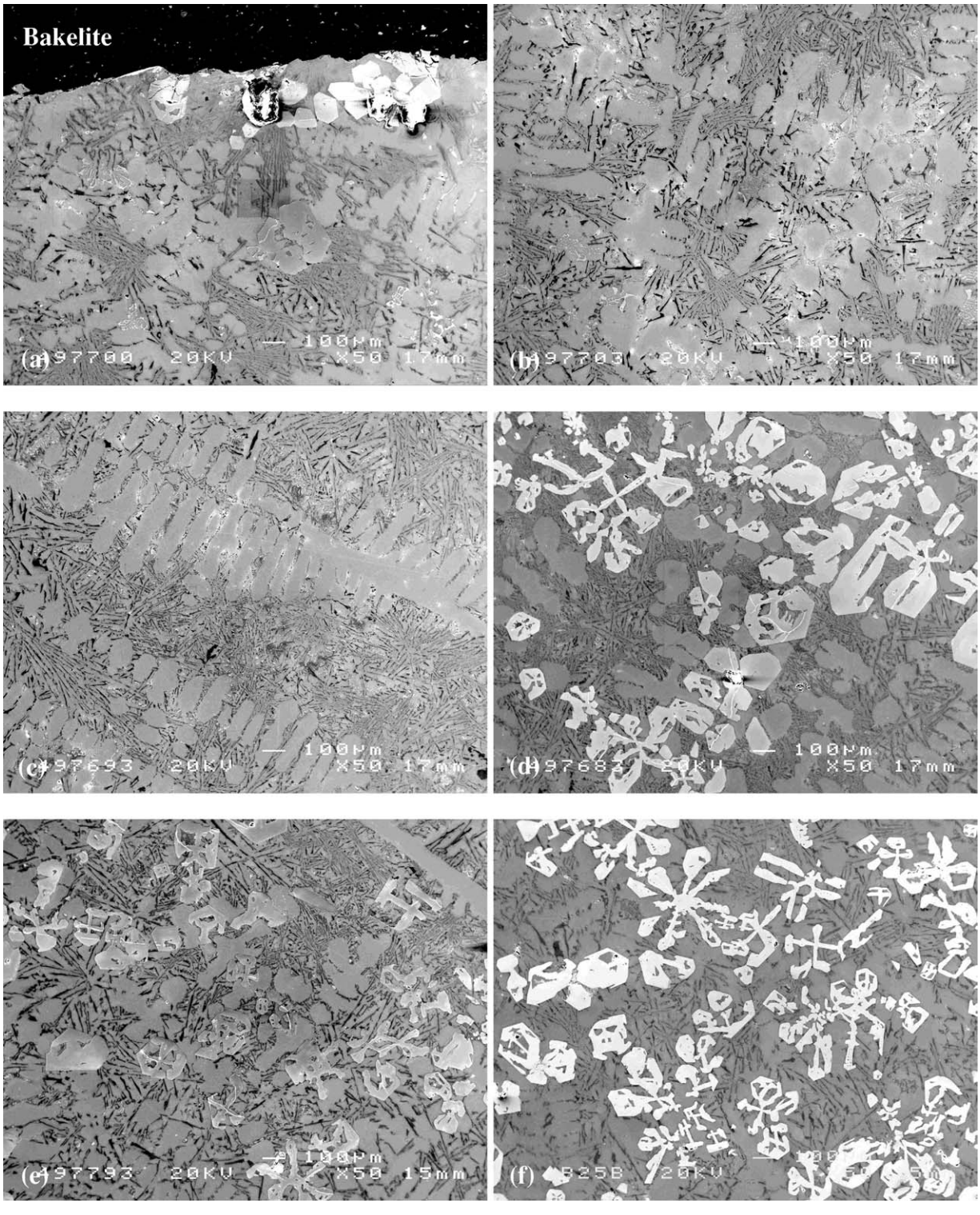

Figure 4 Secondary electron image of Alloy 5 casting sedimented at 600°C for 4 h taken at: (a) the very top, (b) 190 mm, (c) 130 mm, (d) 70 mm, (e) 50 mm and (f) 10 mm from the base of the casting showing the distribution of primary α-Al(FeMn)Si particles.

maximum area of primary α-Al(FeMn)Si phase. Fig. 7a and b show the distribution of the sizes of primary α-Al(FeMn)Si particles along the length of the castings at different original Fe and Mn levels, while Fig. 7c shows the effect of the original IEV on the average sizes of the primary α-Al(FeMn)Si phase in each casting. The variation of particle number per unit area at different heights of the castings is shown in Fig. 8a while Fig. 8b shows the variation with the IEV of the original alloys of the primary particle number for each gram of alloy. The estimated weight of primary α-Al(FeMn)Si phase ("Experimental") and the modelled results using the software programme JMatPro ("Calculated") are shown in Fig. 9. Good agreement was found between the "Experimental" and "Calculated" particle weights except that there was a large deviation for Alloy 5 with a very high original IEV, which may be the result of software or experimental errors. One important reason, of course, is the approximate method used for the estimation of particle weight percentage as stated above. Fig. 10 shows the shape factors (aspect ratio, fullness ratio and roundness) of the primary α-Al(FeMn)Si phase.

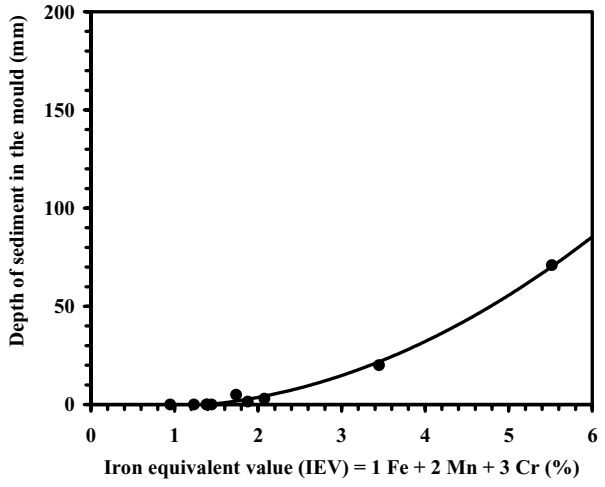

Figure 5 Depth of the sediment at the base of the castings as a function of original iron equivalent value.

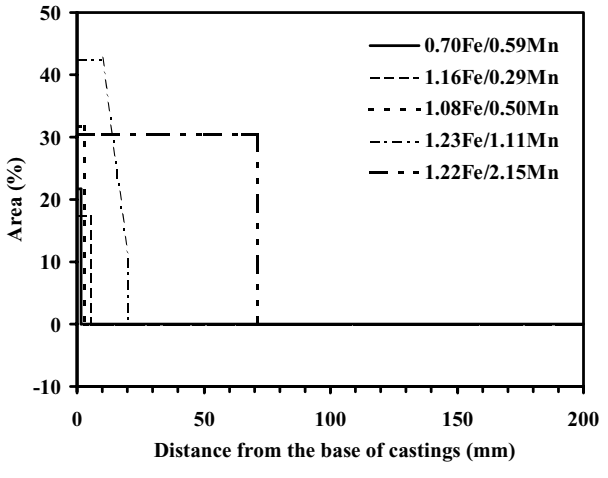

(a)

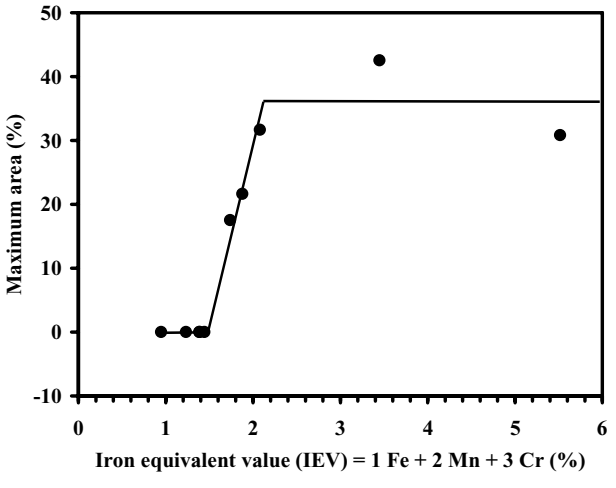

(b)

Figure 6 Effect of original Fe and Mn contents on: (a) average area of primary α-Al(FeMn)Si phase along the length of castings and (b) maximum area.

Fig. 11 shows the variation of Fe and Mn contents along the length of the castings after sedimentation. Table II lists the calculated (using JMatPro) and actual compositions of precipitate-free castings. Fig. 12 contrasts the actual and calculated removal efficiency of Fe and Mn elements. Table III shows the calculated and measured compositions of primary α-Al(FeMn)Si phase.

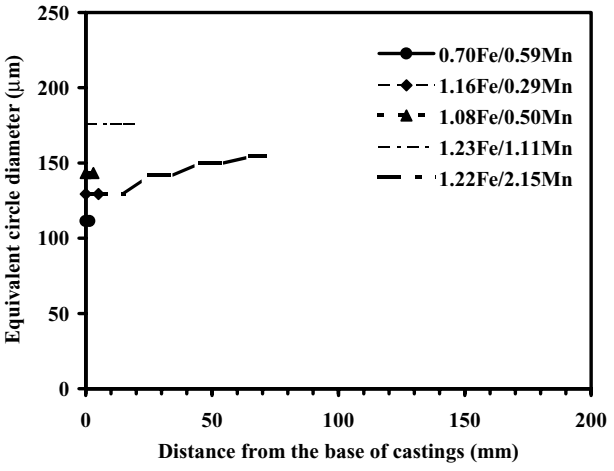

(a)

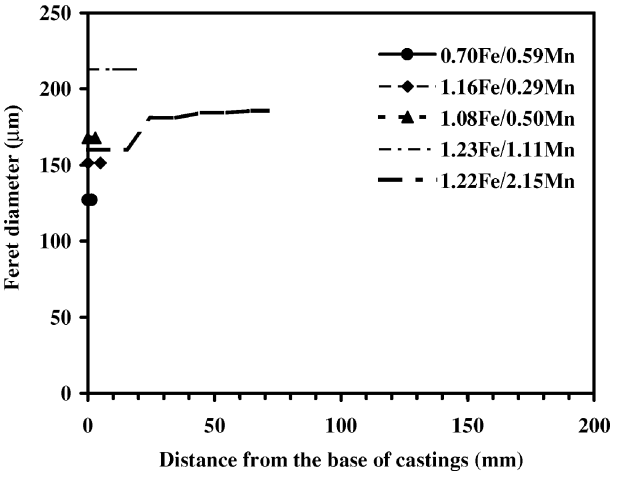

(b)

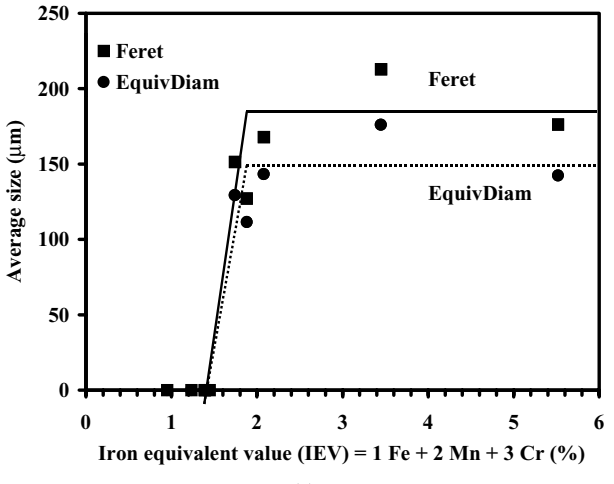

(c)

Figure 7 (a) Equivalent circle diameter and (b) feret diameter quantifying the effect of original Fe and Mn contents on the sizes of primary α-Al(FeMn)Si particles, and (c) average equivalent circle and feret diameters as a function of the original IEV.

4. Discussion

4.1. Convection-free technique

The experimental set-up was specially designed to suppress the natural convection that would naturally occur in a melt and to investigate the influence of Fe and Mn contents on the precipitation and sedimentation of primary α-Al(FeMn)Si particles.

Liquid metal usually experiences natural convection during holding as a result of density differences within

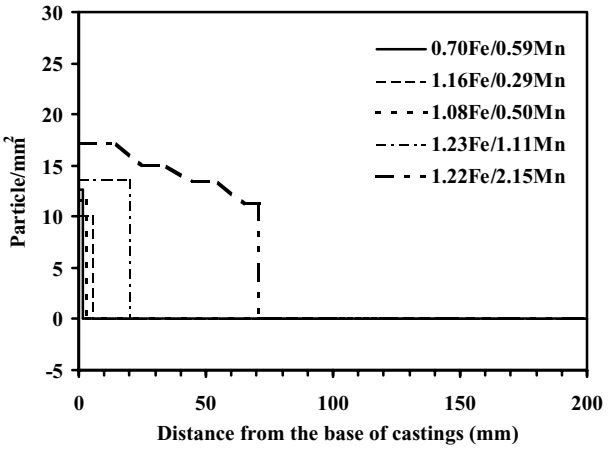

(a)

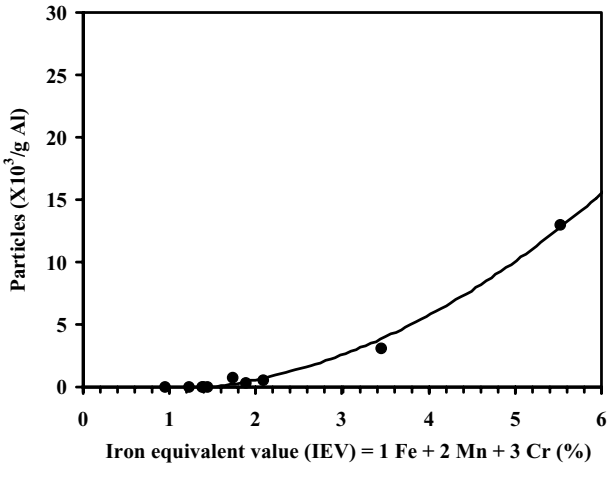

(b)

Figure 8 (a) Effect of Fe and Mn contents on particle number per unit area along the length of castings and (b) effect of the IEV in original alloys on the particle number per gram of alloy.

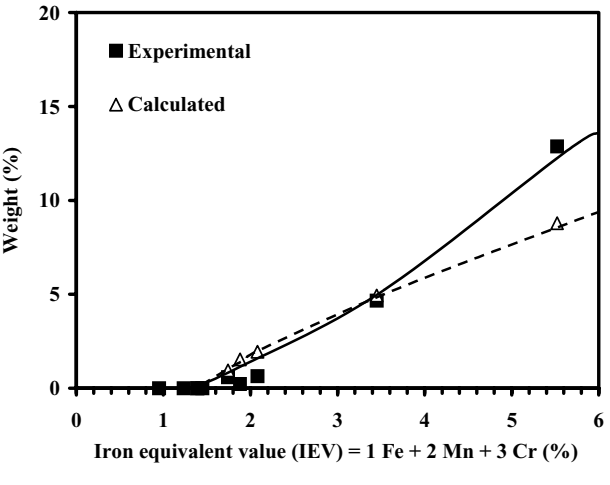

Figure 9 Experimental and calculated (using JMatPro) ratio of weight of primary α-Al(FeMn)Si particles to total metal weight as a function of original iron equivalent value (%).

the liquid that result from differences in temperature and/or composition [18]. Very small temperature gradients will provide a significant driving force for liquid convection because of the low viscosity of the liquid. The vigour of convective mixing is measured by the dimensionless Rayleigh number Ra.

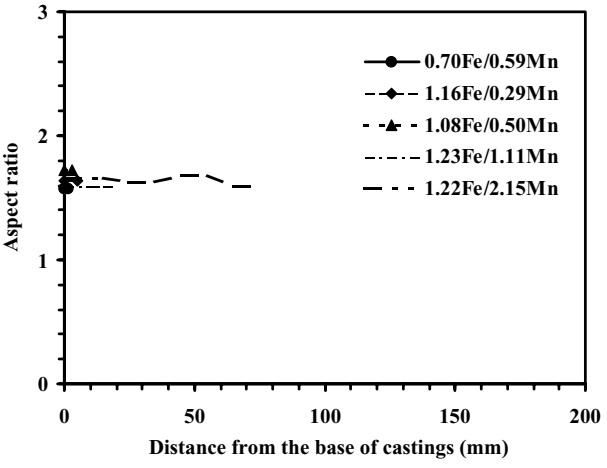

(a)

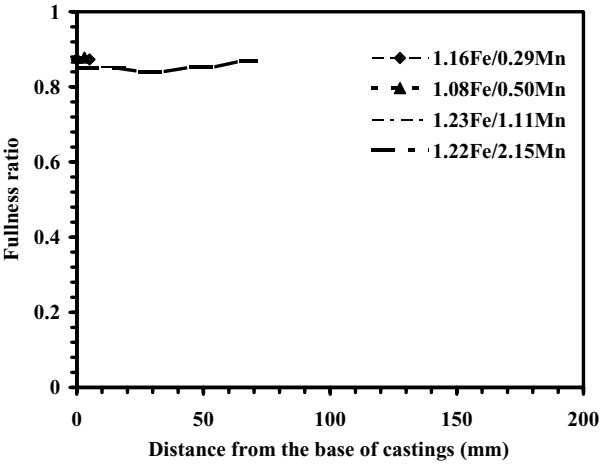

(b)

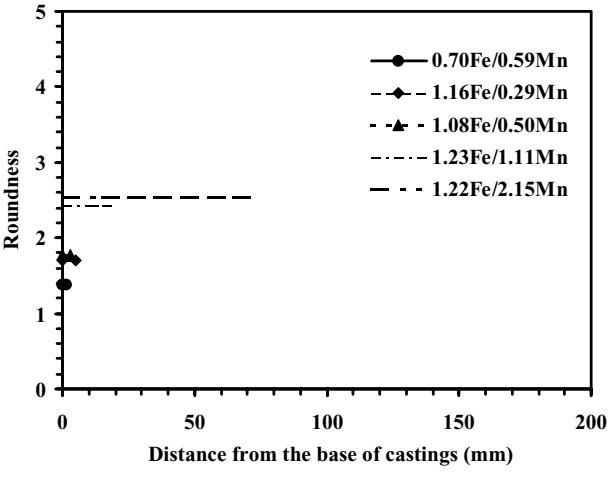

(c)

Figure 10 Effect of original Fe and Mn contents on the shape factors (aspect ratio, fullness ratio and roundness) of primary α-Al(FeMn)Si particles.

The Rayleigh number is defined as the product of the Grashof and Prandtl numbers. The Grashof number is a dimensionless group, which represents the ratio of the buoyancy forces to the viscous forces in free convection. The Prandtl number, which is the ratio of molecular momentum diffusivity and thermal diffusivity, assesses the relation between velocity and temperature distributions [19]. Liquid metals generally have a high thermal conductivity and a small specific heat;

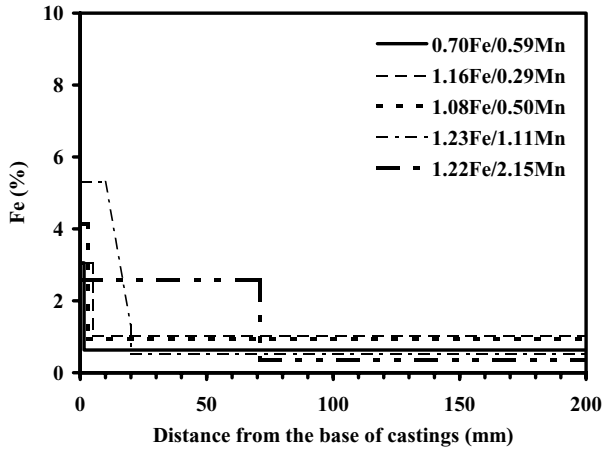

(a)

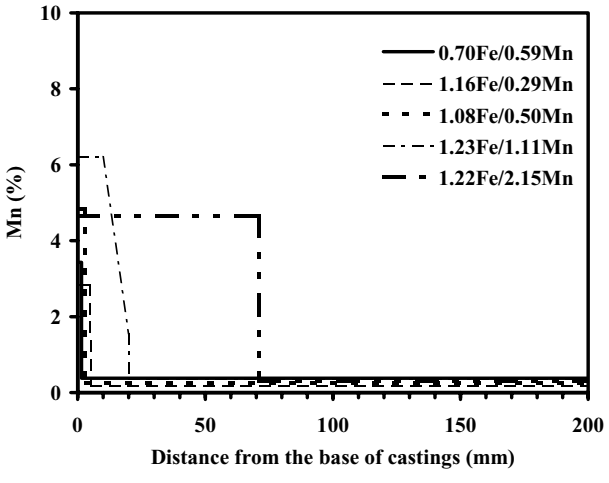

(b)

Figure 11 Effect of original Fe and Mn contents on (a) Fe distribution and (b) Mn distribution in the castings along the length of castings after convection-free sedimentation.

their Prandtl numbers are therefore small, ranging from 0.003 to 0.06 [20].

The Grashof number is defined as

$$Gr = \frac{g\beta\Delta TL^3}{\nu^2}, \tag{1}$$

and the Prandtl number is defined as

$$p_{\mathrm{r}} = \frac{\mu c_{\mathrm{p}}}{\kappa} = \frac{\nu}{\alpha}, \tag{2}$$

Therefore,

$$Ra = GrP_{\mathrm{r}} = \frac{\rho g\beta\Delta TL^3}{\mu\alpha}, \tag{3}$$

where ρ is density of the fluid, kg/m^3; g is acceleration due to gravity, m/s^2; β is thermal expansion coefficient (temperature coefficient of volume expansion), K^{-1}; ΔT is temperature difference, K; L is length along a heat flow path or a characteristic length of a body, m; μ is absolute viscosity (dynamic viscosity), N s/m^2; ν is kinematic viscosity (momentum diffusivity), m^2/s; α is thermal diffusivity, $\alpha = \frac{\kappa}{C_{\mathrm{p}}\rho}$, m^2/s; κ is thermal conductivity, W/m K; C_{p} is specific heat at constant pressure, J/kg K.

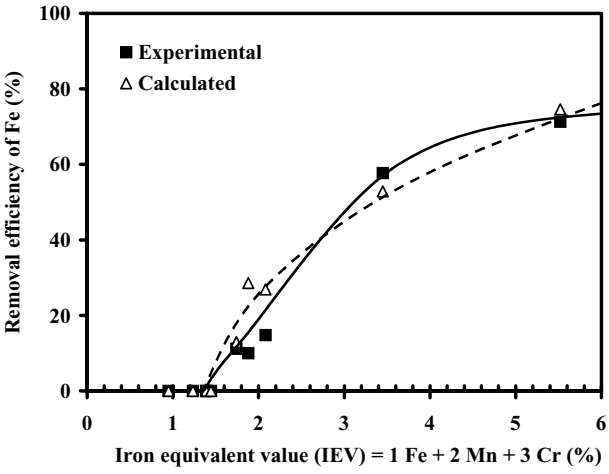

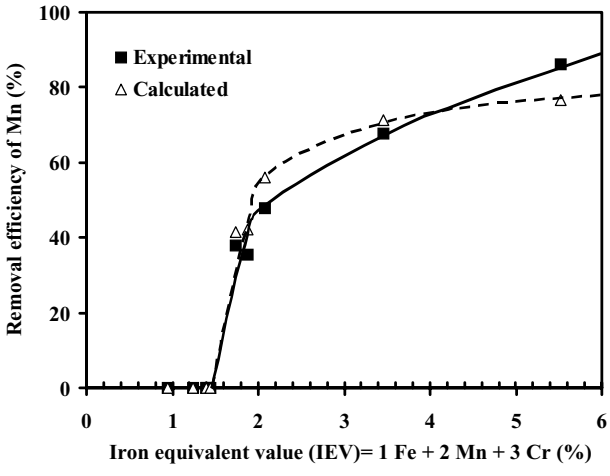

Figure 12 Contrast of actual and calculated (using JMatPro) removal efficiency of Fe and Mn.

Effectively, the Rayleigh number assesses the complex balance between the temperature gradient driving buoyancy, and damping effects of the thermal conductivity of the fluid dissipating thermal differences, and the viscosity. For an unconfined system (such as one comprising a small cooled vertical plate in an infinite liquid), laminar flow occurs for $Ra \leq 10^8$, and turbulent flow occurs above this value [19].

The convection in the current experimental geometry corresponds more closely to that within an enclosure. To be technically precise, it is similar to that in a horizontal cavity non-extensive in the horizontal direction [18]. The critical Rayleigh numbers Ra_{c} is bounded between two values, Ra_{cp} and Ra_{ci}. The greater of the two, Ra_{cp}, applies to the case of a perfectly conducting wall; and the lesser, Ra_{ci}, applies to the case of an adiabatic wall. For the circular cylinder ($\phi 20 \times 200$ mm) in the experimental set-up with an inside diameter $D =$ 20 mm, height $L = 200$ mm, as $D/L = 0.1 \rightarrow 0$, thus $Ra_{\mathrm{cp}}(D/L)^4 \rightarrow 3456$ and $Ra_{\mathrm{ci}}(D/L)^4 \rightarrow 1086$ [20], therefore, $Ra_{\mathrm{cp}} \rightarrow 3.5 \times 10^7$ and $Ra_{\mathrm{ci}} \rightarrow 1.1 \times 10^7$.

The exact thermophysical data for the experimental alloy at 600°C is not available. Thus the values listed in Table IV are the calculated values using JMatPro and that applied to A356 alloy. Substituting these values into Equation 3 yields the critical temperature differences, ΔT, for the case of the perfectly conducting wall, $\Delta T = 33$°C; and for the case of the adiabatic wall, $\Delta T = 10$°C.

TABLE II Calculated (using JMatPro) and actual compositions of precipitate-free castings (wt%)

	Si		Mg		Fe		Mn		Al
	Modeled	Actual	Modeled	Actual	Modeled	Actual	Modeled	Actual	Bal.
Alloy 1	11.33	11.15	0.39	0.40	0.5	0.63	0.34	0.38	Bal.
Alloy 2	11.62	11.52	0.37	0.39	1.01	1.03	0.17	0.18	Bal.
Alloy 3	11.55	12.04	0.36	0.39	0.79	0.92	0.22	0.26	Bal.
Alloy 4	12.09	11.66	0.41	0.55	0.58	0.52	0.32	0.36	Bal.
Alloy 5	11.96	11.78	0.38	0.37	0.31	0.35	0.50	0.30	Bal.

TABLE III Calculated and measured compositions of primary α-Al(FeMn)Si phase

	Si	Fe	Mn	Al	Note
Alloy 1 (wt%)	8.67	13.31	16.74	Bal.	Calculated using JMatPro
Alloy 2 (wt%)	8.48	16.93	13.16	Bal.	Calculated using JMatPro
Alloy 3 (wt%)	8.56	15.56	14.53	Bal.	Calculated using JMatPro
Alloy 4 (wt%)	8.70	13.75	16.31	Bal.	Calculated using JMatPro
Alloy 5 (wt%)	8.87	10.70	19.32	Bal.	Calculated using JMatPro
Average (wt%)	8.66	14.05	16.01	Bal.	Calculated using JMatPro
Average (at%)	9.87	8.06	9.33	Bal.	Calculated using JMatPro
Measured (at%)	9.65	7.22	12.51	Bal.	References [6, 8]

TABLE IV Thermophysical data of experimental alloys at 600°C

Constant	Values	Note
ρ	2463 kg/m^3	Calculated using JMatPro
ρ_p	3378.7 kg/m^3	Calculated using JMatPro
β	1.46×10^{-4}/K	Calculated using JMatPro
μ	1.19×10^{-3} N s/m^2	A356 at 700°C [21]
ν	4.8315×10^{-7} m^2/s	Calculated from μ and ρ
κ	80.1 W/m K	Calculated using JMatPro
C_p	1458 J/kg K	Calculated using JMatPro[a]
g	9.81 m/s^2	

Note: The physical properties of the base alloy were calculated based on the medium range of the composition specification, except for Fe, the maximum value.

[a]The C_p value is sensitive to the amount of primary α-Al(FeMn)Si particles. The reported value was calculated considering the formation of primary α-Al(FeMn)Si particles. The C_p value for the liquid metal at 600°C is estimated to be 1110 J/kg K.

If the temperature difference in the melt is below these critical values, natural convection will be expected to be completely suppressed. In addition to the geometrical constraint provided by the narrow tubular mould, the copper die was deliberately chosen to reduce temperature differences in the melt. These were observed in practice to be no more than ±3°C. Therefore, the present experiment was predicted to be a robust convection-free design.

Clearly, the occurrence of convection during sedimentation will influence, or even reverse the settling of oxides and primary α-Al(FeMn)Si particles, particularly films and small particles. During the convection-free conditions, the primary α-Al(FeMn)Si particles have fully settled to the bottom of the mould as shown in Figs 3 and 4. In addition, the oxide films were also found to have sedimented to the base of castings (Fig. 3). Some primary α-Al(FeMn)Si particles were observed on or near the mould wall (Fig. 2) or near the very top of the castings (Fig. 4a) possibly because of the hindrance of oxide films attached to the mould wall or the liquid surface. The effectively full sedimentation of primary α-Al(FeMn)Si particles facilitated the quantifying of the primary intermetallics.

4.2. Influence of Fe and Mn on the sedimentation of primary α-Al(FeMn)Si particles

The precipitation and sedimentation of primary α-Al(FeMn)Si phase was observed at 600°C in all experimental alloys. This has been supported by the calculated Gibbs energy parameters using JMatPro for the experimental alloys at 600°C (Table V). The calculated compositions of primary α-Al(FeMn)Si phase as shown in Table III are consistent with the measured compositions for an alloy similar to Alloy 1 [6, 8].

With the increase of the original IEV there are increases in the precipitated particle weight (Fig. 9) and the number of primary α-Al(FeMn)Si particles (Fig. 8), indicating that high Fe and Mn in the original cast Al–Si alloys is, as expected, favourable for the formation of primary α-Al(FeMn)Si phase. The results from Alloys 2–5 at approximately 1.2% Fe level indicate that higher Mn content in the original alloys greatly favours the formation of primary α-Al(FeMn)Si phase at a given Fe level (Figs 8 and 9).

With the increase of the original IEV it is expected that there will be an increase in the depth of sediment as shown in Fig. 5. Both the area of sediment (Fig. 6) and the particle size (Fig. 7) similarly increase. However, there is some evidence that further increase of the original IEV from about 3.5 causes a decrease in maximum volume fraction (Fig. 6b) and size (Fig. 7c) of primary α-Al(FeMn)Si particles. The effect may be merely the result of experimental error; the results possibly being a plateau beyond IEV $\approx$ 2. Alternatively, particle coarsening may be playing a part.

It is interesting to note that maximum volume fraction of primary α-Al(FeMn)Si particles after 4 h has reached 42.6% (Fig. 6). This is significantly lower than the loose random packing area percentage of 59.3% for uniform spheres [22]. These low packing densities corroborate

TABLE V Calculated data of thermodynamics using JMatPro for the experimental alloys at 600°C

Alloys	Partial Gibbs energy of each element (J/g)					Activity of each element					Enthalpy H (J/g)	Entropy S (J/g K)	Gibbs energy G (J/g)	C_p (J/g K)
	Al	Si	Mg	Fe	Mn	Al	Si	Mg	Fe	Mn				
1	−307.96	−2347.79	−46366.83	−111362.5	−91489.26	0.96	0.72	0.00168	2.18E−07	3.36E−06	1056.87	2.6651	−1270.12	1.4543
2	−343.41	−2167.92	−46608.2	−106227.9	−96503.74	0.95	0.74	0.00163	4.42E−07	1.69E−06	1059.79	2.6698	−1271.38	1.4227
3	−331.95	−2191.02	−46960.85	−108048.7	−94478.88	0.96	0.74	0.00155	3.44E−07	2.23E−06	1050.11	2.6603	−1272.71	1.4424
4	−389.22	−1734.4	−46178.11	−110657.9	−92074.16	0.59	0.79	0.00173	2.40E−07	3.10E−06	1019.18	2.6342	−1280.88	1.4548
5	−373.92	−1801.89	−46631.86	−115301.8	−88957.56	0.95	0.78	0.00162	1.27E−07	4.77E−06	972.73	2.5934	−1291.74	1.4330

the picture that the Fe-rich sediment is laced through with oxide films from which the entrapped liquid slowly escapes as from a slowly collapsing sponge. This is the picture first seen by Mountford and Calvert in their ultrasonic studies of sedimentation in aluminium melts [23].

The large particles would be expected to settle first at the bottom of the castings, the small particles arriving later at the top of the sediment because the settling velocity is proportional to the square of particle diameter. However, the larger Fe-rich particles are found at the top of the precipitate-rich metal for Alloy 5 (Fig. 7a and b). One reason may be that the top particles have better access to Fe and Mn diffusing from the open liquid above to feed their growth and coarsening behaviour. During the slow consolidation of the spongy deposit under its own weight, minute jets of liquid would be expected to be forced out of the top of the mass. Such microjects would mix the bulk liquid above the sediment, increasing the advection of solutes to the upper layers. Conversely, the particles lower down in the sediment would have no access to additional solute apart from that due to dissolving smaller particles as part of the natural coarsening process [7, 8].

It is interesting to evaluate the effect of the concentration of primary α-Al(FeMn)Si particles on their sedimentation velocity since this may be considerably less than the terminal falling velocity under free settling conditions where the effects of mutual interference are negligible. The overall result is that, in a concentrated suspension, the large particles are retarded and the small ones accelerated [24]. In the case of Alloy 5 the average equivalent circle diameter of the primary α-Al(FeMn)Si particles is approximately 142 μm (Fig. 7c). The sedimentation can be dealt with approximately according to a model for coarse particles with uniform sizes (The division between coarse and fine particles is somewhat arbitrary but is at the order of 100 μm) [24].

When the concentration of coarse particles and wall effect are considered, the sedimentation velocity of uniform spherical particles in a liquid at any voidage e in a vessel of diameter d_t can be calculated from the following equations [24]:

$$u_c = \frac{\mu}{\rho d}\left(2.33G_a^{0.018} - 1.53G_a^{-0.016}\right)^{13.3} \times \left(1 + 2.4\frac{d}{d_t}\right)^{-1} e^n \quad (4)$$

$$G_a = \frac{d^3\rho(\rho_p - \rho)g}{\mu^2} \quad (5)$$

where G_a is the Galileo number, u_c is sedimentation velocity of particles in suspension, μ is absolute viscosity (dynamic viscosity) of the liquid, ρ is density of liquid, ρ_p is density of particles, g is gravitational acceleration, d is diameter of the sphere or equivalent spherical diameter, d_t is diameter of tube or vessel, e is voidage of suspension ($e = 1 -$ fractional volumetric concentration), and n is an index determined by following formula:

$$\frac{4.8 - n}{n - 2.4} = 0.043G_a^{0.57}\left[1 - 2.4\left(\frac{d}{d_t}\right)^{0.27}\right] \quad (6)$$

Using parameter values in Table IV, and $d = 142$ μm, $d_t = 20$ mm, $e = 0.70$ for Alloy 5 sedimented at 600°C for 4 h (the fractional volumetric concentration for Alloy 5 is approximately 0.30 as shown in Fig. 6), we suppose that primary α-Al(FeMn)Si particles could sediment to the concentration quickly to check the consequent consolidation at this concentration. Thus we can obtain $G_a = 44.736$ and $n = 4.508$ calculated from Equations 5 and 6, respectively. The sedimentation velocity of particles in suspension for Alloy 5 is approximately 1.37 mm/s calculated from Equation 4. In contrast, the free settling velocity for same size particle (142 μm) calculated from Stokes' law is approximately 8.46 mm/s indicating that the sedimentation velocity of the concentrated primary particles decreases by approximately 5 times. However, despite this lower rate, the particles still only take approximately 2.5 min to settle to the bottom of the mould. The low volume fraction of primary α-Al(FeMn)Si particles for Alloy 5 (approximately 30%) in the sediment seems to suggest that some other factors may dominate their falling behaviour. The presence of oxide films and their random attachment to the narrow mould walls or the very top surface of the melts may be the uncontrolled factor. Although thicker films may add to weight, tending to make descent faster, their larger area will more than counter this, greatly slowing their fall. Furthermore, the oxide films floating in the liquid metal may be somewhat inflated and opened by the precipitation of hydrogen during holding at 600°C, conferring some buoyancy. Primary α-Al(FeMn)Si particles randomly distributed on or very close to the stainless steel wall (coated with boron nitride) or the very top surface of the melt (Figs 2 and 4a) appear to "hang" in these positions, sometimes with no obvious sign of support since on the metallographic sections they appear detached from the wall and from each other. This is to be expected if the particles are deposited on, and therefore attached to, extensive, but thin films that are difficult to see in section as a result of their

extreme thinness. The largest films are expected to have dimensions of mm or even cm, and thus are a significant fraction of the size of the mould. Random attachment is therefore to be expected, slowing or even preventing the sedimentation of primary α-Al(FeMn)Si particles. Further complication arises because of the likelihood of agglomeration and entanglement of films and particles during sedimentation.

In addition to the technical difficulties of characterising the process itself, the lack of reliable, and reasonably accurate, analytical techniques to measure and quantify oxide films in cast aluminium alloys has greatly hindered the understanding of the removal efficiency of oxide films from aluminium melts. At the moment, therefore, it is not clear how much Fe and Mn contents are required for the most effective removal of the films.

The sedimentation of primary α-Al(FeMn)Si particles causes, of course, the removal of Fe and Mn from the top, precipitate-free portion of melts as shown in Fig. 11. It was also found that the actual chemical compositions and removal efficiency of Fe and Mn elements are reasonably consistent with the modelled results using JMatPro (Table II and Fig. 12). It is interesting to find that the experimental alloys (Al-11.5Si-0.4Mg originally containing 0.7–1.22Fe and 0.3–2.15Mn) have approximately a fixed content of 0.3% Mn but varied Fe contents after the convection-free sedimentation at 600°C (Fig. 11). It seems that there is an equilibrium Mn content corresponding to a precipitation temperature for a given alloy. The removal effectiveness for Mn is higher than that for Fe as shown in Fig. 12. For instance, approximately 71.6% Fe and 86% Mn have been removed from Al-11.5Si-0.4Mg-1.22Fe-2.15Mn alloy (Alloy 5) after sedimentation at 600°C. With the increase of the IEV in the original alloys, the removal of Fe and Mn also tends to increase (Fig. 12) but there is a diminishing efficiency of return at higher original IEVs. The results for Alloys 2–5 at approximately 1.2% Fe indicate that higher Mn contents in the original alloys favour the removal of Fe and Mn.

5. Conclusions

1. The convection-free experimental design in the work appears to be successful in suppressing the occurrence of natural convection during the sedimentation of primary α-Al(FeMn)Si compounds and oxide films. In the narrow tube mould, however, some oxide films can adhere to the mould wall or the very top melt surface, hindering some sedimentation near the walls. Otherwise, so far as could be determined, almost all primary α-Al(FeMn)Si particles in the bulk melts and some oxide films appear to settle out fully.

2. The precipitated weight of primary α-Al(FeMn)Si phase is mainly determined by Fe and Mn contents in the original alloys at a given precipitation temperature. With an increase of the iron equivalent value (IEV) or of the ratio of Mn/Fe at a given Fe level in the original alloys there are increases in the precipitated weight, and in the number and size of primary α-Al(FeMn)Si particles. The particle volume fraction and depth of sediment in the mould also increase with IEV or the ratio of Mn/Fe at a given Fe level. However, a further increase of IEV above 3.5 may cause a slight decrease in particle volume fraction and size. The apparent effect may be a result of experimental error, the volume fraction and size of particles possibly reaching a plateau beyond IEV $\approx$ 2.

3. After sedimentation there exists an equilibrium Mn content corresponding to a precipitation temperature for a given alloy. In Al-11.5Si-0.4Mg alloy originally containing 0.7–1.22Fe and 0.3–2.15Mn, this Mn content is approximately 0.3% after sedimentation at 600°C. The removal efficiency of Fe and Mn increases with the IEV of the original alloy or the ratio of Mn/Fe at a given Fe level. The sedimentation process removes Mn with a higher efficiency than Fe. For instance, approximately 71.6% Fe and 86% Mn have been removed from Al-11.5Si-0.4Mg-1.22Fe-2.15Mn alloy.

4. The success of JMatPro in calculating phase equilibria and relevant thermophysical and physical properties, suggests that the modelling route could be used to explore different alloys where sedimentation was feasible during processing.

Acknowledgements

The authors would like to thank Professors I. R. Harris and M. H. Loretto for the provision of facilities in the School of Metallurgy and Materials and the IRC in Materials at the University of Birmingham, UK. One author (XC) would also like to thank the committee of Vice Chancellors for the award of an Overseas Research Students Scholarship. Many thanks are also due to Drs J-P Immarigeon and M Jahazi for their invaluable review of this manuscript.

References

1. J. CAMPBELL, "Casting" (Butterworth-Heinemann, Oxford, 1991) p. 1.
2. *Idem.*, *Foundry Manag. Techn.* **2** (2001) 26 .
3. J. R. DAVIS, "ASM Speciality Handbook: Aluminium and Aluminium Alloys" (ASM International, 1993) p. 199.
4. D. APELIAN, in "Advances in Aluminium Casting Technology," Rosemont, Illinois, USA, Oct. 12–15, 1998, edited by M. Tiryakioglu and J. Campbell, p. 153.
5. X. CAO and J. CAMPBELL, *AFS Trans*. **108** (2000) 391.
6. *Idem.*, *Int. J. Cast Metals Res.* **13**(3) (2000) 175.
7. *Idem.*, *AFS Trans.* **109** (2001) 501.
8. X. CAO, in PhD Thesis, The University of Birmingham, United Kingdom, 2001.
9. X. CAO and J. CAMPBELL, in "Materials Solutions 2002—Advances in Aluminium Casting Technology II," Columbus, OH, USA, Oct. 7–10, 2002 (ASM International) p. 135.
10. *Idem.*, *Int. J. Cast Metals Res.* **15** (2003) 595.
11. *Idem.*, *Metallurg. Mater. Trans.* **34A** (2003) 1409.
12. *Idem.*, *ibid.* to appear in 2004.
13. J. L. JORSTAD, *Die Cast. Engng.* (Nov./Dec. 1986) 30.
14. A. S. OSIO, S. LIU and D. L. OLSON, *Mater. Sci. Engng.* **221** (1996) 122.
15. E. E. UNDERWOOD, "Quantitative Stereology" (Lockheed-Georgia Company, Marietta, Georgia, 1970) p. 88.
16. N. SAUNDERS, X. LI, A. P. MIODOWNIK and J.-PH. SCHILLÉ, in "Materials Design Approaches and Experiences," edited by J.-C. Shao (TMS, Warrendale, PA, 2001) p. 185.
17. *Idem.*, in "Modeling of Casting, Welding and Advanced Solidification Processes X," edited by D. Stefanescu *et al.* (TMS, Warrendale, PA, 2003) p. 669.

18. W. M. ROHSENOW, J. P., HARTNETT and E. N. GANIC, in "Handbook of Heat Transfer Fundamentals," 2nd ed. (McGraw-Hill Book Co., 1985) p. 6.41.
19. F. KREITH, "Principles of Heat Transfer," 2nd ed. (International Textbook Co., Scranton, PA, 1965) p. 326.
20. S. KAKAC and Y. YENER, "Convective Heat Transfer," 2nd ed. (CRC Press Inc., Boca Raton, Florida, 1995) p. 302, 311.
21. AUBURN UNIVERSITY, Metal Alloy Thermophysical Data, Http://metalcasting.auburn.edu/data.html (2000).
22. R. M. GERMAN, "Particle Packing Characteristics" (Metal Powder Industries Federation, Princeton, NJ, 1989) p. 89.
23. N. D. G. MOUNTFORD and R. CALVERT, *J. Inst. Metals* **88** (1959/60) 121.
24. J. M. COULSON, J. F. RICHARDSON, J. R. BACKHURST and J. H. HARKER, "Chemical Engineering-Particle Technology and Separation Processes," 4th ed., Vol. 2 (Pergamon Press Plc., England, 1991) p. 14, 95.

Received 5 August 2003
and accepted 6 January 2004